The Journal of Experimental Biology 210, 4379-4389
Published by The Company of Biologists 2007
doi:10.1242/jeb.009787

Routine turning maneuvers of koi carp *Cyprinus carpio koi*: effects of turning rate on kinematics and hydrodynamics

Guanhao Wu[1,*], Yan Yang[2,3] and Lijiang Zeng[1]

[1]*State Key Laboratory of Precision Measurement Technology and Instruments, Department of Precision Instruments, Tsinghua University, Beijing 100084, China,* [2]*The Laboratory for Biomechanics of Animal Locomotion, Graduate University of Chinese Academy of Sciences, Beijing 100049, China and* [3]*Department of Modern Mechanics, University of Science and Technology of China, Hefei 230026, China*

*Author for correspondence (e-mail: tophow99@mails.tsinghua.edu.cn)

Accepted 16 October 2007

Summary

Spontaneous swimming behaviors of koi carp *Cyprinus carpio koi* were recorded using a video tracking system. Routine single-beat turns were selected from the recorded image sequences for kinematic and hydrodynamic analysis. As with C-starts, the turns can be divided into two stages (stage 1 and stage 2), based on kinematics. Stage 1 involves a bend to one side forming a C-shaped curve in the body, while stage 2 corresponds to the return flip of the body and tail. The turning angle in stage 1 accounts for the greatest portion of the total turning angle and the mean turning rate in stage 1 reflects the intensity of turn. The effects of the turning rate in stage 1 on both kinematics and hydrodynamics were examined. The duration of stage 1 remained relatively stable over a nearly tenfold change in turning rate. Consequently, the turning angle is dominated by the turning rate in stage 1. The turning radius is not related to the swimming speed. Moreover, except in very fast turns, the turning radius is also not affected by the turning rate. The angle between the side jet and the carp's initial orientation of a turn does not change substantially with the turning rate, and it is always close to 90° (94.2±3.1°, *N*=41), so the orientation of the side jet in the forthcoming turn can be predicted. The angle between the jet and the line joining the center of mass of the carp and the trailing edge of the tail (mean value in stage 1) is also always close to 90° (95.3±1.3°, *N*=41). It is helpful for the carp to maximize the torque so as to improve the turning efficiency. In stage 1, the impulsive moment obtained from the beat of the body and tail and the mean angular momentum of the carp show an agreement in magnitude. Two types of flow patterns in the wake of routine single-beat turns are revealed. The difference between the two types of wakes is in whether or not a vortex ring and a thrust jet are generated in stage 2. The recoil speed of the tail, the bending amplitude of the turn, and the angle of attack of the tail are three probable factors influencing the flow patterns in stage 2.

Key words: routine turn, single-beat turn, kinematics, particle image velocimetry, hydrodynamics, wake, koi carp, *Cyprinus carpio koi*.

Introduction

Fish swimming behaviors can generally be divided into steady swimming and maneuvers. So far, most studies of fish swimming have focused on the kinematics (Ferry and Lauder, 1996; Donley and Dickson, 2000) and hydrodynamics (Müller et al., 1997; Müller et al., 2001; Nauen and Lauder, 2002; Tytell and Lauder, 2004) of steady swimming or on kinematics while examining rapid maneuvering [i.e. fast starts (Domenici and Blake, 1997; Spierts and Leeuwen, 1999; Domenici et al., 2004)]. However, watching fish swimming in nature reveals that most fishes rarely swim steadily or perform fast maneuvers; instead, they frequently perform some moderate maneuvers (Webb, 1991; Wu et al., 2007). Routine turning maneuvers (spontaneous turns), in particular, are key elements of such moderate maneuvers. Due to complications and difficulties in quantification, routine turning maneuvers have not received detailed attention (Webb and Fairchild, 2001).

Routine turning maneuvers can be divided into median and/or paired fins (MPF) turns and body and/or caudal fin (BCF) turns, according to the propulsion patterns of fish (Webb, 1998; Gerstner, 1999). Experimental studies of the two types of turns have traditionally focused on the kinematics and maneuverability (Gerstner, 1999; Budick and O'Malley, 2000; Walker, 2000; Webb and Fairchild, 2001). In recent years, digital particle image velocimetry (DPIV) has been employed to investigate the flows generated by the fish performing BCF turns (Wolfgang et al., 1999; Sakakibara et al., 2004) or MPF turns (Drucker and Lauder, 2001). Drucker and Lauder studied the wake dynamics of MPF turns in bluegill sunfish in detail and clarified the hydrodynamic mechanism of MPF turns (Drucker and Lauder, 2001). However, the quantitative analysis in experimental hydrodynamics of BCF turns has not yet been well documented. Furthermore, the empirical relationship between kinematics and hydrodynamics remains yet an unstudied aspect of BCF turns.

Examining the changes in kinematics (Jayne and Lauder, 1995; Donley and Dickson, 2000) and hydrodynamics (Drucker and Lauder, 2000; Nauen and Lauder, 2002; Tytell, 2004) over a range of speeds is an effective way to study steady swimming of fish. Changing the swimming speed of the fish in these experiments was accomplished by controlling the flow speed in the flume. Unfortunately, it is extremely difficult to force fish to turn at a precisely controlled and repeatable speed and/or turning rate. Webb studied the influences of swimming speed and acceleration on turning radius by placing fish in predation situations (Webb, 1983). However, the effect of speed and/or turning rate has not been examined when studying the kinematics and hydrodynamics of spontaneous turns of fish.

A video tracking system for simultaneous measurements of kinematics and flow of a freely swimming fish (Wu et al., 2006; Wu et al., 2007) offers a suitable approach to studying spontaneous maneuvers of fish. In the present study, we employ this method to quantify the kinematics and flow patterns of koi carp *Cyprinus carpio koi* performing routine BCF turns. As reported elsewhere (Gerstner, 1999), routine BCF turns include cruising turns and single-beat turns. In our experiments, single-beat turns occurred much more frequently than cruising turns, and the sample size of cruising turns was small. Consequently, only the single-beat turns were considered in the present study. The selected single-beat turns cover a large range of turning rates and linear regressions were used to analyze the effects of turning rate on kinematics and hydrodynamics. Furthermore, two types of flow patterns generated in routine single-beat turns were characterized, and the related kinematics was analyzed.

Materials and methods

Experimental animals and procedures

The experiments were carried out on koi carp *Cyprinus carpio koi* L. The carp swam individually in a working volume (50 cm×25 cm×10 cm) of a glass tank (100 cm×40 cm×30 cm) at a water temperature of 25±2°C. The working volume was confined by wire grids covered with fine mesh. Spontaneous swimming behaviors of each carp were recorded by two cameras mounted on a translation stage that was controlled so as to track the carp. One of the cameras (Camera C, MTV-1881EX; 25 frames s^{-1}, 768 pixels×576 pixels; Mintron Inc., Taipei, China) was used to obtain the kinematic data of the carp; because it was in interlaced scanning mode, we obtained 50 images s^{-1} by dividing and interpolating the recorded frames. The other was a high-speed camera (HSC, AM1101; 100 frames s^{-1}, 640 pixels×480 pixels; Joinhope Ltd, Beijing, China), was used to obtain the flow field around the carp. The experimental setup and procedures were as previously described (Wu et al., 2006; Wu et al., 2007).

Kinematics

Each image from camera C was binarized by using a custom-made computer program. After clearing the stray points, we programmed applications to obtain the midline and the geometric center of the carp. The geometric center was approximately treated as the center of mass (COM). We define the body axis x' (Fig. 1) as the linear regression line through the points at the anterior half (from nose to the middle) of the midline. It indicates the heading of the carp. The change in orientation of axis x' was defined as the turning angle (β in Fig. 1) of the carp. The lateral excursion of the tail tip (d in Fig. 1) was calculated as distance between x' axis and the tail tip on the midline. Its maximum value, d_{max}, represents the bending amplitude of the carp during a turn. Turning radius (R_t) was defined as the radius of the trajectory of COM during a turn. The moving speed of the carp at the onset of a turn was denoted by U_0, and was calculated based on the displacement of the COM.

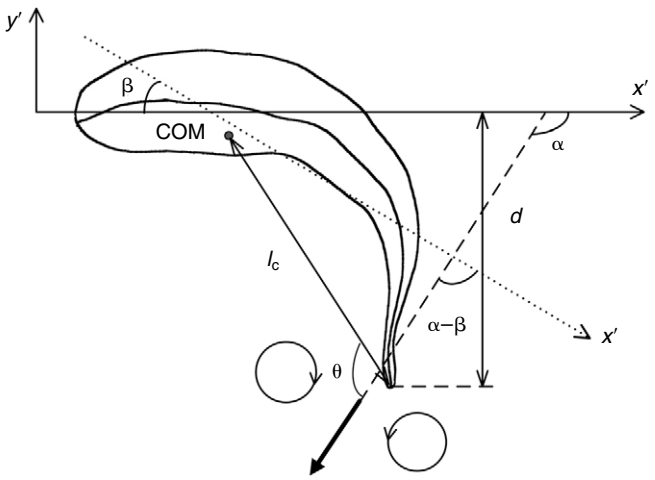

Fig. 1. The coordinate system and notation used to describe the kinematics and the wake of the fish. Two counter-rotating circles represent a pair of vortices. The bold arrow indicates the jet flow. The dotted line indicates the body axis of the carp at the onset of a turn. The broken lines are auxiliary lines. See text for more details and List of symbols and abbreviations for definitions.

Like C-start escape responses (Weihs, 1972), routine single-beat turns can also be divided into two main stages, based on kinematics (stage 1 and stage 2). Stage 1 involves a bend to one side, causing a C-shaped curve in the body, while stage 2 corresponds to the return flip of the body and tail. Duration of stage 1 (t_1) was defined as the time between the onset of bend and the onset of return flip of the tail. Duration of stage 2 (t_2) was defined as the time between the end of stage 1 and the instant when the return flip finished. Besides the kinematic variables given above, turning angles (β_1, β_2), mean turning rates (ω_1, ω_2) and net changes of speed (ΔU_1, ΔU_2) were used to characterize the kinematics of a routine single-beat turn. The subscripts of the symbols indicate which stage the variables are used for. β_1 always has a positive sign. The sign of β_2 is positive if the rotation in stage 2 is in the same direction as that in stage 1; otherwise, it is negative. The sign convention for ω_1 and ω_2 is similarly defined. ΔU_1 and ΔU_2 were calculated by considering only the magnitude of the moving speed of the carp. When the tail beats in water, it is held at an angle (angle of attack) to its line of motion (Bainbridge, 1963). In the present study, the angle of attack of the tail was only considered for the region at the tail tip. This angle at the beginning, the middle and the end of stage 2 were denoted by ϕ_{2b}, ϕ_{2m} and ϕ_{2e}, respectively.

Hydrodynamics

The velocity and vorticity fields of the flow were obtained using an 'mpiv' toolbox (Mori and Chang, 2004). The

interrogation window we used was 24 pixels×24 pixels (4.1 mm×4.1 mm), and the overlap between two consecutive windows was 50%. The velocity field was filtered and smoothed by the functions in the 'mpiv' toolbox.

To estimate the momentum shed by a carp during turning, we used the vortex ring model (Milne-Thomson, 1966) and assumed that all the energy shed by the carp is contained in oval-shaped vortex rings. Illuminating a cross section through such a ring should yield a flow pattern consisting of two vortices of opposite rotational senses (Fig. 1). Locations of the vortices were determined by plotting the contours of vorticity. The momentum of a vortex ring can be expressed (Tytell and Lauder, 2004) as:

$$I = \tfrac{1}{4}\pi\rho\bar{\Gamma}hD\ , \quad (1)$$

where ρ is the density of fresh water, $\bar{\Gamma}$ is the mean absolute value of the circulations (Γ) of the pair of vortices, h is the height of the ring, equivalent to the tail's height, and D is the diameter in the plane of the light sheet. Circulation Γ is the line integral of the tangential velocity component about a curve enclosing the vortex. The momentum I in stages 1 and 2 are denoted by I_1 and I_2, respectively. The angle α between the jet flow and x' (Fig. 1), namely the jet angle, indicates the direction of the momentum of the vortex ring. The jet angles in stages 1 and 2 is denoted as α_1 and α_2, respectively. Jet angle α_1 was determined at the end of stage 1, by which time paired vortices were fully developed. Jet angle α_2 was determined at the end of stage 2.

To estimate the impulsive moment obtained from the beat of the body and tail in stage 1 (L_{i1}), we defined two parameters, distance l_c and angle θ (Fig. 1). l_c is the distance between the COM of the carp and the trailing edge of the tail, while θ is the angle between the jet and the line through the COM of the carp and the trailing edge of the tail. Both l_c and θ were considered as the mean values in stage 1. L_{i1} can be estimated as:

$$L_{i1} = I_1 l_c \sin\theta\ . \quad (2)$$

To compare with L_{i1}, we estimated the mean angular momentum of the carp in stage 1 (L_{j1}). It can be obtained from:

$$L_{j1} = (J_1 + J_{a1})\omega_1\ , \quad (3)$$

where J_1 is the mean moment of inertia of the carp in stage 1, and J_{a1} is the mean added moment of inertia of entrained liquid in stage 1. Following Sakakibara et al. (Sakakibara et al., 2004), the moment of inertia of the carp (J) was estimated based on the assumption that the density is homogeneous throughout the carp's body. In estimating the added moment of inertia of entrained liquid (J_a), we assumed that the body of the carp was a flattened ellipsoid. The semi-major axis (a) of the ellipsoid was considered to be equal to half the distance from the nose to the tail tip of the carp, the horizontal semi-minor axis (b) was assumed to be equal to half the maximum width of the carp, and the vertical semi-minor axis (c) was assumed to be equal to half the maximum height of the carp. Based on the assumptions above, J_a can be calculated (Saunders, 1957):

$$J_a = k\,(\tfrac{4}{15}\rho\pi abc)\,(a^2 + b^2)\ , \quad (4)$$

where k is the coefficient of added moment of inertia and ρ is the density of water.

Statistical analysis

Sigma Stat (Systat Software Inc., Point Richmond, CA, USA) software was used for statistical analyses. The individuals we selected were similar in body size, so we expected no differences in the kinematic and hydrodynamic variables among the individuals; this was confirmed by one-way analysis of variance (ANOVA). Regressions were performed on the kinematic and hydrodynamic variables to examine the effects of turning rate. We also used one-way ANOVA to compare the kinematic variables of the turns with two different types of wakes. All data are presented as means ± s.e.m. (standard error).

Results

Kinematic and hydrodynamic data were taken from five individuals, of mean body length (L) 56.6±1.0 mm (N=5), mass 2.6±0.2 g (N=5) and fineness ratio 3.96±0.05 (N=5). From the fineness ratios, we used the coefficient of added moment of inertia k as 0.608 (Saunders, 1957). According to the recorded swimming sequences, 41 single-beat turns were selected by two criteria: (1) the quality of particle images were high enough to yield a high density of original velocity vectors in the wake; (2) the shadow created by the body and caudal peduncle was visible (to make sure the body and caudal fin moved through the light sheet). Mean turning rates in stage 1 (ω_1) of the 41 turns covered a range from 88 to 1050 deg. s^{-1}, and were divided into four turning rate categories: slow (0–200 deg. s^{-1}), moderate (200–400 deg. s^{-1}), fast (400–600 deg. s^{-1}) and very fast (>600 deg. s^{-1}). The sample sizes of the four categories indicate that slow and moderate routine turns occur more frequently than fast and very fast routines turns when the koi carp are swimming spontaneously (Fig. 2).

Individual effects on all the kinematic and hydrodynamic variables were examined by one-way ANOVA. In all cases, no significant difference was found among the individuals (P>0.2).

Kinematics

As shown in Fig. 3A, the turning angle in stage 1 (β_1) had a significant linear relationship with the mean turning rate in stage 1 (ω_1) (r^2=0.887, P<0.001; Table 1), while the turning angle in stage 2 (β_2) did not (r^2=0.063, P=0.114; Table 1). Obviously, β_1 was always much greater than β_2 in magnitude (Table 1), indicating that the changes in heading were mainly accomplished in stage 1 when the carp performed a routine single-beat turn. Thus the mean turning rate in stage 1 (ω_1)

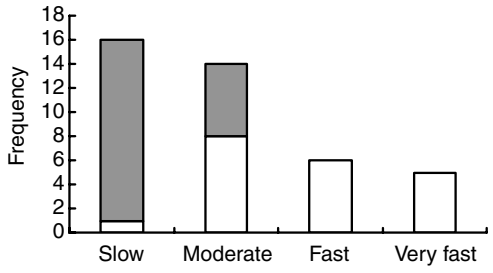

Fig. 2. Frequency distributions of the routine single-beat turns in the four turning categories. Open bars, turns with type I wake; filled bars, turns with type II wake. The sum of the two bars represents the total number of turns in each category.

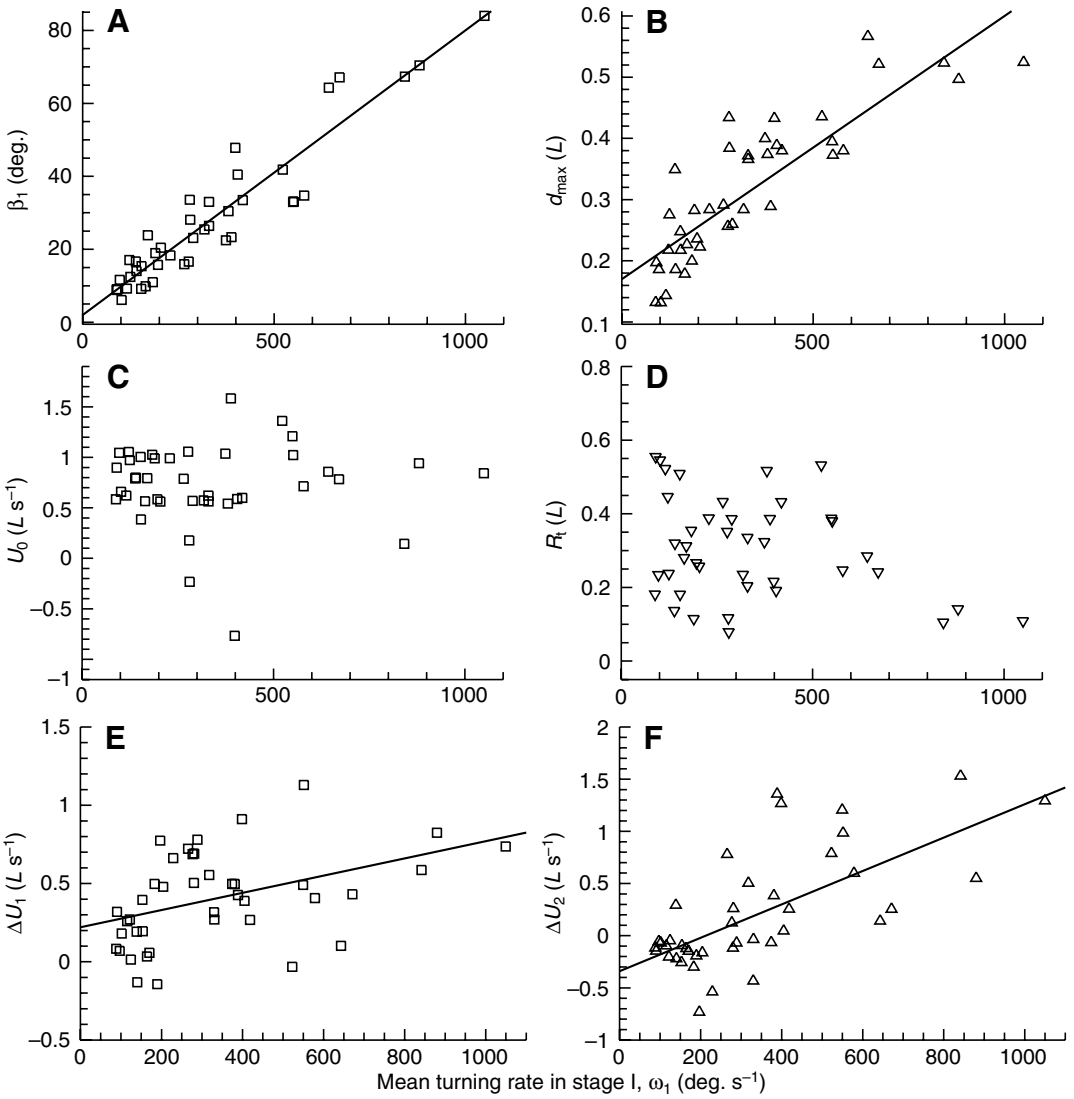

Fig. 3. Mean turning rate in stage 1 (ω_1) plotted against (A) the turning angle in stage 1 (β_1), (B) the bending amplitude (d_{max}), (C) the moving speed at the onset of a turn (U_0), (D) turning radius (R_t), (E) net change of speed in stage 1 (ΔU_1) and (F) net change of speed in stage 2 (ΔU_2). In A,B,E,F, linear regression lines are shown as solid lines (see text and Table 1 for regression coefficients and *P* values). No significant linear relationship exists in C and D and so a regression line is not shown.

reflected the intensity of the whole turn, which is why we examine the effects of ω_1 instead of the turning rate of the whole turn. The duration of stage 1 (t_1) seemed to remain stable in the single-beat turns with different ω_1 (P=0.125). Consequently, β_1 was dominated by ω_1. The duration of stage 2 (t_2) and the mean turning rate in stage 2 (ω_2) also did not seem to be affected by ω_1 significantly (P=0.09 and P=0.135, respectively). In addition, the relationship between the bending amplitude (d_{max}) and ω_1 was examined (Fig. 3B, Table 1). The faster the carp turned, the more tightly its body bent.

The moving speeds of the carp at the onsets of the turns (U_0) covered a range from –0.76 to 1.58 $L\,s^{-1}$ (Fig. 3C), and they showed very poor relationship with ω_1 (r^2=0.00007, P=0.958). However, both the net changes of speed in stage 1 and stage 2 (ΔU_1 and ΔU_2) showed significant linear relationship with ω_1 (Fig. 3E,F, Table 1). The turning radii of the turns (R_t) covered a range from 0.08 to 0.55 L (Fig. 3D). The relationship between R_t and U_0 was examined by using linear regression and no significant relationship was found (P=0.157). In addition, the relationship between R_t and ω_1 was marginally non-significant (P=0.066). However, when ω_1 was greater than 600 deg. s^{-1}, namely in the very fast category, the turning radii distributed in a relatively narrow range and were relatively smaller than those of the turns with lower turning rates (Fig. 3D). Hence, we considered the slow, moderate and fast categories as one group and the very fast category as another group. Significant differences were found in the turning radius between the two groups (P=0.023).

Hydrodynamics

Two types of wakes were found when the carp performed routine single-beat turns: wake type I (Fig. 4) and wake type II (Fig. 5). Fig. 4 gives a two-dimensional view of the type I wake. The start and stop vortices in this plane indicated the formation

Table 1. *Linear regressions of the kinematic and hydrodynamic variables against the turning rates in stage 1*

	N	Constant	Slope	r^2	*P*
Kinematics					
β_1 (deg.)	41	2.0±1.8	0.078±0.004	0.887	<0.001
β_2 (deg.)	41	3.5±0.9		0.063	0.114
t_1 (s)	41	0.087±0.004		0.059	0.125
t_2 (s)	41	0.156±0.011		0.072	0.09
ω_2 (deg. s^{-1})	41	13.5±5.3		0.057	0.135
d_{max} (L)	41	0.17±0.02	$(4.3±0.4)\times10^{-4}$	0.743	<0.001
U_0 (L s^{-1})	41	0.73±0.06		0.00007	0.958
ΔU_1 (L s^{-1})	41	0.22±0.07	$(5.5±1.8)\times10^{-4}$	0.183	0.005
ΔU_2 (L s^{-1})	41	–0.34±0.11	$(1.6±0.3)\times10^{-3}$	0.475	<0.001
R_t (L)	41	0.30±0.02		0.084	0.066
Hydrodynamics					
I_1 (10^{-5} N s)	41	$(1.9±1.8)\times10^{-5}$	$(5.5±0.4)\times10^{-7}$	0.807	<0.001
α_1 (deg.)	41	98±6	0.07±0.01	0.374	<0.001
α_1–β_1 (deg.)	41	94.2±3.1		0.004	0.680
l_c (L)	41	0.616±0.005	$(-7.5±1.2)\times10^{-5}$	0.511	<0.001
θ (deg.)	41	95.3±1.3		0.056	0.136
$(J_1+J_{a1})/(J_1+J_{a1})_{max}$*	41	0.934±0.007	$(-2.6±0.2)\times10^{-4}$	0.856	<0.001
L_{i1} (10^{-6} Nm s)	41	$(1.1±0.6)\times10^{-6}$	$(1.7±0.2)\times10^{-8}$	0.748	<0.001
L_{j1} (10^{-6} Nm s)	41	$(0.9±1.6)\times10^{-7}$	$(9.4±0.4)\times10^{-9}$	0.933	<0.001
$(L_{i1}–L_{j1})/L_{i1}$	41	0.52±0.03		0.0255	0.318
I_2 (10^{-5} N s)	20	$(-5.5±5.4)\times10^{-5}$	$(6.5±1.0)\times10^{-7}$	0.706	<0.001
α_2 (deg.)	20	44±7	–0.038±0.014	0.302	0.012

Only the overall mean value is listed for non-significant regressions. *P* values are for the effect of turning rate.
*$(J_1+J_{a1})_{max}$ is the maximum value of (J_1+J_{a1}) during a turn, estimated when the carp took a straight posture.
See List of symbols and abbreviations for definitions.

and evolvement of the vortex rings. When the carp started to bend, suction and pressure flows formed a bound vortex (vortex 1 in Fig. 4B) around the inflection points of the body. At the same time, the suction flow at the caudal peduncle induced another vortex (vortex 2 in Fig. 4B). When the tail reached the maximum excursion and recoiled subsequently, the two vortices shed and formed a vortex pair in the wake (Fig. 4C,D). The jet between the two vortices, named side jet, was directed nearly laterally, so the momentum must help the carp to turn. During the recoil of the body and tail, another suction flow was formed at the caudal peduncle and two more vortices (vortices 3 and 4) were induced (Fig. 4D). At the end of stage 2, vortices 3 and 4 shed and formed another vortex pair (Fig. 4E,F). The jet between the two vortices, so-called thrust jet, had a considerable rearward component. In comparison with the wake of type I, only one vortex pair (vortices 1 and 2 in Fig. 5) was visible in the wake of type II. The vortex pair was generated in stage 1 (Fig. 5B–D) while no substantial vortices were formed in stage 2 (Fig. 5D–F). Consequently, in the wake of type II, only the side jet was substantial and the thrust jet was missing. Only some weak flow moved following the tail in stage 2 (Fig. 5D–F).

The frequencies of wake type I and wake type II appeared to increase and decrease, respectively, with the increasing turning rate (Fig. 2). Fast and very fast turns generated type I wakes; type II wakes appeared frequently in slow and moderate turns. We examined the kinematic variables that might affect, or might be affected by, the wake types (Table 2). A probable factor influencing the wake type was the recoil speed of tail (d_{max}/t_2). It turned out that the recoil speeds of the tail in turns with wake type I were much greater than those in the turns with wake type II (P<0.001; Table 2). Bending amplitude (d_{max}), which determined the recoil amplitude of tail, was another probable factor influencing the flow patterns. The bending amplitudes in the turns with wake type I were much greater than those in the turns with wake type II (P<0.001; Table 2). The angle of attack of the tail at the beginning of stage 2 (ϕ_{2b}) did not show significant differences between the turns with the two types of wakes (P=0.497; Table 2), but the angle of attack of the tail at the middle and the end of stage 2 (ϕ_{2m} and ϕ_{2e}) did (P=0.002 and P<0.001, respectively; Table 2). The differences in the angle of attack of the tail might also result in differences in the generated flows. The initial speed, U_0, showed no significant

Table 2. *Comparisons of the kinematics of the turns with the two types of wakes*

	Wake type I	Wake type II	*P*
d_{max}/t_2 (L s^{-1})	3.68±0.27	1.36±0.09	<0.001
d_{max} (L)	0.40±0.02	0.24±0.02	<0.001
U_0 (s^{-1})	0.72±0.12	0.74±0.05	0.62
ΔU_2 (L s^{-1})	0.64±0.11	–0.2±0.04	<0.001
ϕ_{2b} (deg.)	10.3±1.2	11.9±0.9	0.497
ϕ_{2m} (deg.)	37.9±2.5	22.9±1.3	0.002
ϕ_{2e} (deg.)	65.8±2.6	27.5±3.7	<0.001
N	20	21	–

See List of symbols and abbreviations for definitions.
Values are means ± s.e.m. (*P* calculated by one-way ANOVA).

difference in the turns with two types of wakes (P=0.62). However, due to the thrust jet, the net changes of speeds in stage 2 (ΔU_2) in the turns with wake type I were significantly greater than those in the turns with wake type II (P<0.001). In stage 2, the speed of the carp increased 0.64±0.11 L s^{-1} (N=20) with the thrust jet but decreased 0.2±0.04 L s^{-1} (N=21) without the thrust jet.

The effects of turning rate on hydrodynamics were examined in the same way as those in kinematics. The momentum of the vortex ring shed in stage 1 (I_1) and the corresponding jet angle (α_1) both increased linearly with the mean turning rate (ω_1) in stage 1 (Table 1, Fig. 6A), but the angle (α_1–β_1), namely the angle between the side jet and the carp's initial orientation of a turn (see α–β in Fig. 1), remained stable when the mean turning rate increased (P=0.68; Table 1). This indicates that, before a carp performs a routine single-beat turn, the orientation of the side jet generated in the forthcoming turn can be estimated. As described above in *Kinematics*, the bending

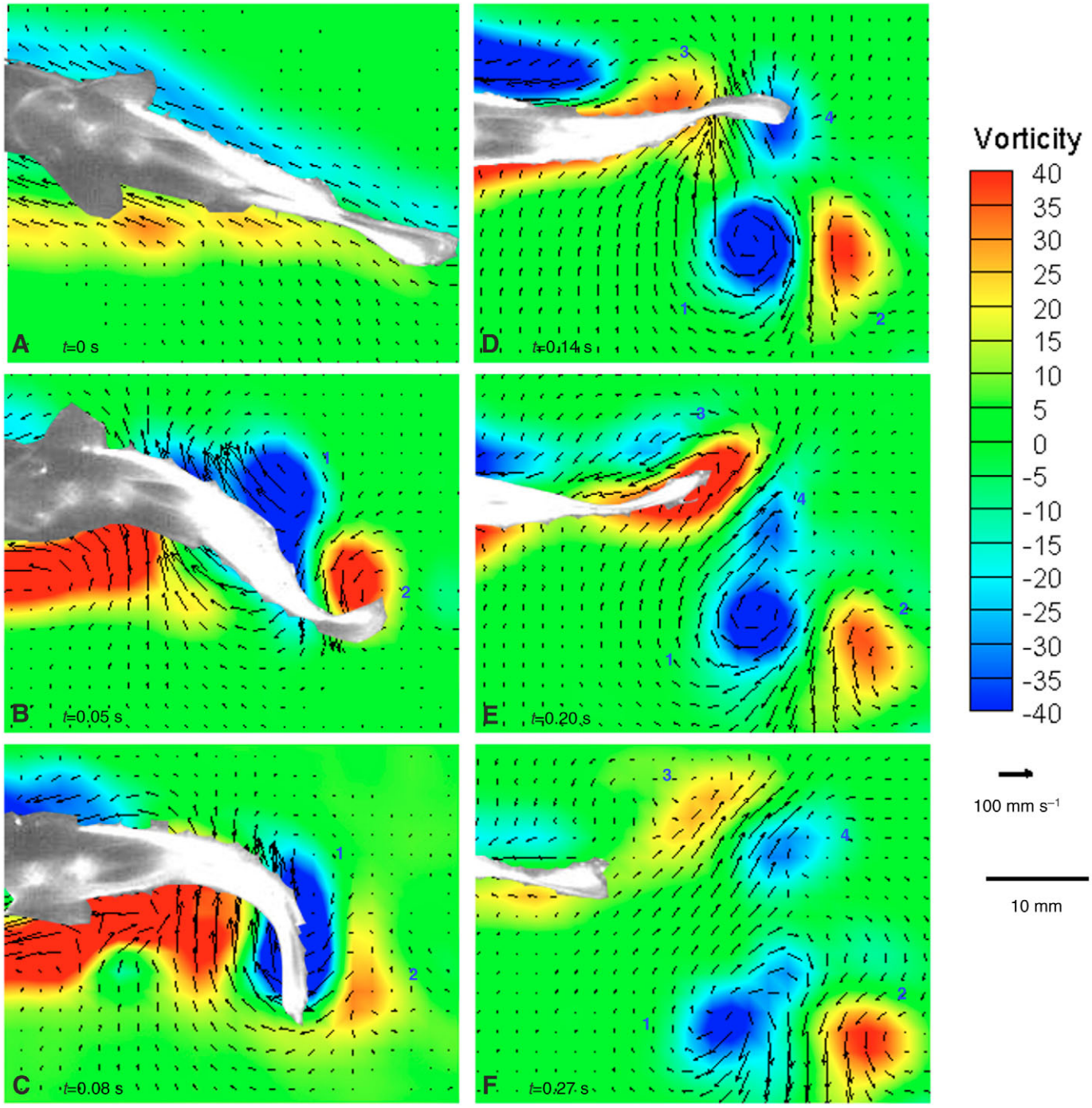

Fig. 4. Representative flow patterns of wake type I. Black arrows represent flow velocity magnitude and direction, and vortices are numbered. Vorticity is shown in color in the background. (A–F) Evolvement of vorticity and flow velocity vector fields at different times during the turn.

amplitude increased with the turning rate, so that the distance from the COM to the trailing edge of the tail (l_c) and J_1+J_{a1} (normalized such that the maximum value of J_1+J_{a1} during a turn was unity) decreased linearly with the increasing ω_1 (r^2=0.856, P<0.001; Table 1). However, the angle θ between the jet and the line joining the COM of the carp and the trailing edge of the tail remained stable when the turning rate increased (P=0.136; Table 1). In routine single-beat turns with various turning rates, θ was close to 90° (θ=95.3±1.3°, N=41). This is favorable for maximizing the impulsive moment and improving the turning efficiency according to Eqn 2. The impulsive moment obtained from the beat of the body and tail in stage 1 (L_{i1}) and the mean angular momentum of the carp in stage 1 (L_{j1}) both increased linearly with increasing ω_1 (Table 1, Fig. 6B), but the slope of L_{i1} was greater than that of L_{j1}. L_{i1} was always greater than L_{j1}, and (L_{i1}–L_{j1}) mainly reflected the loss of angular momentum because of the drag and the acceleration reaction. The ratio of (L_{i1}–L_{j1}) to L_{i1} was not affected by ω_1 (P=0.318; Table 1), and its value (0.52±0.03; N=41) indicated that the angular momentum loss caused by drag and the acceleration reaction was a remarkable part of the total angular momentum exerted.

Considering only turns with wake type I, the momentum of the vortex ring shed in stage 2 (I_2) increased linearly with the

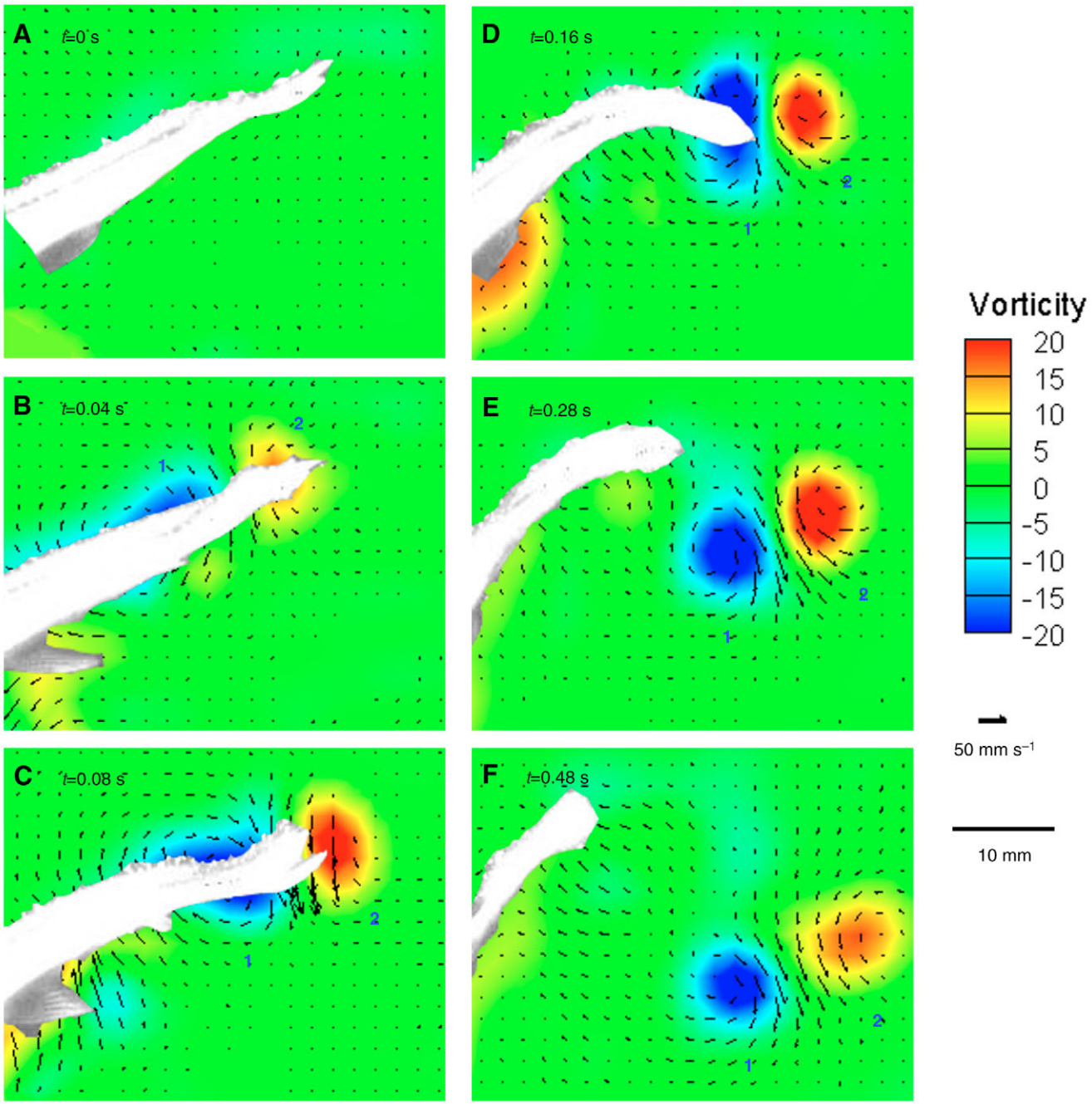

Fig. 5. Representative flow patterns of wake type II. See legend of Fig. 4 for details.

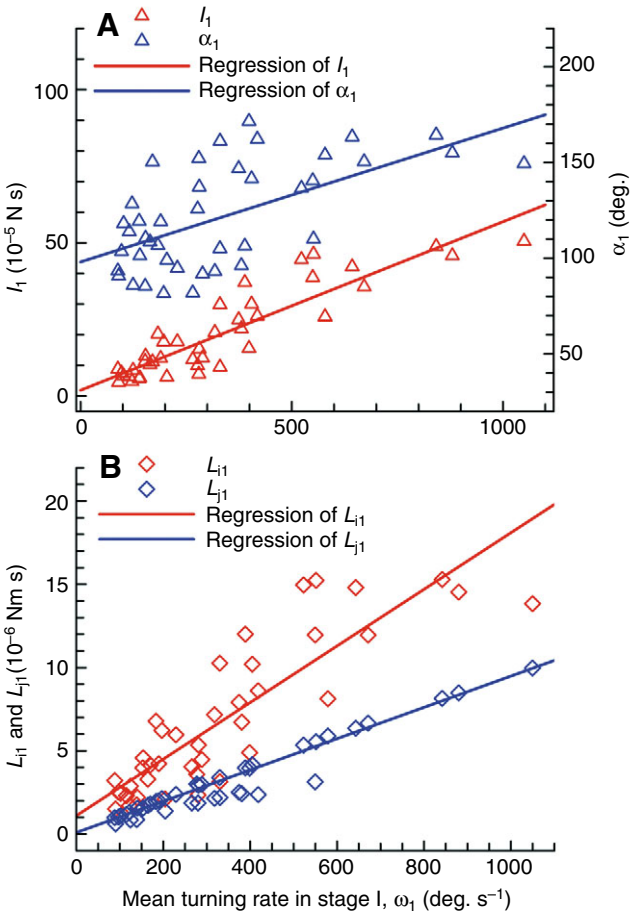

Fig. 6. Linear regressions of mean turning rate in stage 1 (ω_1) plotted against (A) the momentum of the vortex ring (I_1) and the jet angle in stage 1 (α_1) and (B) the impulsive moment obtained from the beat of the body and tail (L_{i1}) and the mean angular momentum (L_{j1}) in stage 1.

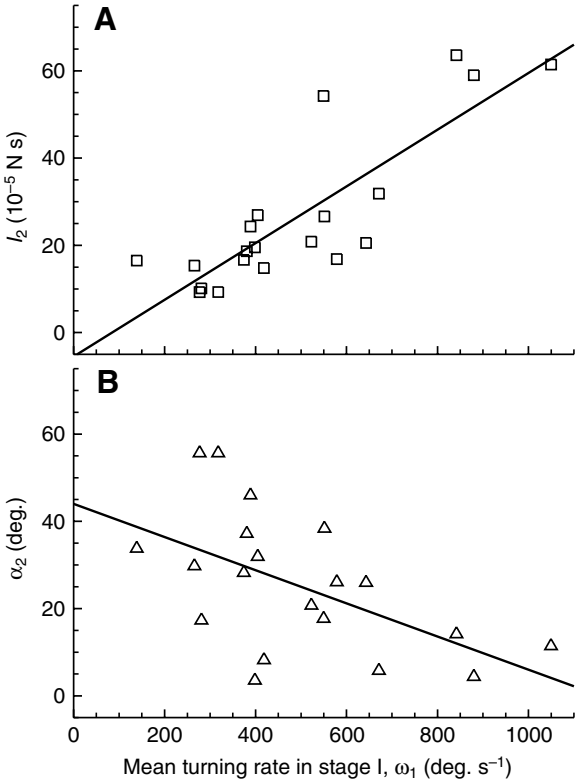

Fig. 7. Linear regressions of mean turning rate in stage 1 (ω_1) plotted against (A) the momentum of the vortex ring shed in stage 2 (I_2) and (B) the jet angle of the vortex ring shed in stages 2 (α_2).

turning intensity while the corresponding jet angle (α_2) decreased linearly (Table 1, Fig. 7A,B). The jet angle (α_2) covered a range from 4° to 56° (Fig. 7B). In most cases, both the lateral and posterior components of the thrust jet were remarkable. With increasing turning intensity, the proportion of the posterior component increased while the proportion of the lateral component decreased.

Discussion

Effects of turning rate on kinematics

It is intriguing to note that the duration of stage 1 in routine single-beat turns of koi carp remains relatively stable over a nearly tenfold change of turning rate. Duration of stage 1 in spiny dogfish (*Squalus acanthias*) decreases with turning rate in slow-escape responses, but is not related to turning rate in fast-escape responses (Domenici et al., 2004). The authors suggested that the differences in the relationship between the duration of stage 1 and the turning rate are possibly subject to neural controls (Domenici et al., 2004). Notice that routine turns in our study are spontaneous, but escape maneuvers of spiny dogfish are stimulated. The causes of the differences between these two types of maneuvers in the relationship between the duration of stage 1 and the turning rate need additional electromyographic studies for clarification.

Previous studies have revealed that the turning radius is not related to the swimming speed in several species of fishes (reviewed by Domenici and Blake, 1997). The same conclusion can be drawn for the koi carp. Moreover, the turning radius is also not affected by the turning rate (except very fast turning rate), in accordance with other studies (Gerstner, 1999). If the slow, moderate and fast categories are considered as one group, however, and the very fast category is considered as another group, the turning radius in the latter group is significantly smaller than in the former. This is probably because the turning rate in the very fast category is close to the magnitude of that in fast-starts, and the turning radii in fast-starts are usually smaller than those in routine turns (Webb and Fairchild, 2001).

Our results show that the turning angle in stage 1 accounts for the greatest portion of the total turning angle of a routine single-beat turn. Moreover, the duration of stage 1 remains stable in various routine single-beat turns. Consequently, the turning angle of a single-beat turn is dominated by the turning rate in stage 1. The moving speeds of the carp at the onset of turns cover a wide range. The appearance of a single-beat turn is not affected by the swimming speed. Moreover, the turning rate of a turn and the swimming speed before the turn are independent; however, the net changes of speed in stage 1 and stage 2 are both shown to have linear relationships with the turning rate in stage 1.

Effects of turning rate on hydrodynamics

The angle between the side jet and the carp's initial orientation of a turn (α_1–β_1) is always close to 90° (94.2±3.1°, N=41), and is substantially independent of the turning rate. The same conclusion can be drawn from escape maneuvers in damsel-fly larvae (*Enallagma cyathigerum* L.) (Brackenbury, 2003), and it means that the orientation of the side jet in the forthcoming turn can be predicted. Another interesting result concerning the side jet is that the angle θ between the jet and the line through the COM of the carp and the trailing edge of the tail is also close to 90° (95.3±1.3°, N=41). It is helpful for the carp to maximize the torque so as to improve the turning efficiency.

In stage 1, the impulsive moment obtained from the beat of the body and tail (L_{i1}) and the mean angular momentum of the carp (L_{j1}) both increased linearly with the increasing turning rate, and the slope of L_{i1} is greater than that of L_{j1} (Fig. 6B). But the ratio of (L_{i1}–L_{j1}) to L_{i1} (0.52±0.03, N=41) remains stable in the turns with a large range of turning rates. The difference between L_{i1} and L_{j1} is rather large, and mainly caused by drag and the acceleration reaction, but may also be affected by direct measurement error and errors in estimation. For instance, (1) the smoothing operations in our flow measurements may reduce the measured circulation (Fincham and Spedding, 1997) and the spatial resolution of our DPIV system is not very high, so that it may contribute to measurement error in estimating circulation. (2) The shape of the vortex ring is not measured precisely, so Eqn 1 is based on the small core vortex ring model, which may not be strictly appropriate (Dabiri, 2005), and therefore may lead to an over- or underestimation of the impulse of flow. (3) As described in the *Hydrodynamics* section of Materials and methods, the moment of inertia of the carp was estimated approximately based on an assumption, which may have led to substantial errors. (4) Additionally, the assumption in estimating the added moment of inertia of entrained liquid will also lead to some errors. Even so, L_{i1} and L_{j1} show an agreement in magnitude in the turns with various turning rates. But to make a more accurate comparison of the two parameters needs more precise measurements and more accurate estimations.

As discussed elsewhere (Wolfgang et al., 1999; Wu et al., 2006), the vortex ring shed in stage 2 helps the fish to accelerate. With the increase in turning intensity, the momentum exerted on the carp in stage 2 increases and the jet angle in stage 2 decreases (tends to zero). Both changes boost the acceleration in stage 2.

Two types of wakes and related kinematics

In steady swimming, several species of fishes change their wakes substantially as they change swimming speed (Nauen and Lauder, 2002; Drucker and Lauder, 2000). At low speeds, bluegill sunfish generate a single vortex ring per fin beat on the downstroke, but at high speeds they generate two on the downstroke and the upstroke (Drucker and Lauder, 2000). In the present study, two types of flow patterns are found in the wake of routine single-beat turns of koi carp *Cyprinus carpio koi*. The difference between the two types of wakes is whether or not a vortex ring and the thrust jet are generated in stage 2. Consequently, the related kinematics shows a large difference between the turns with the types of wakes (i.e. the net change of speed in stage 2). As mentioned above, the spatial resolution of our DPIV system is not very high and may prevent detection of additional vortices in the wake of type I. Referring to the error report of 'mpiv' toolbox' (Mori and Chang, 2004), however, the error of velocity in our flow measurements is about 0.1 mm s^{-1}. Therefore, if a vortex ring does shed in stage 2 but is not detected, it must be much smaller in size, of much weaker vorticity and without thrust jet in comparison with the vortex ring shed in stage 1. In this case, the conclusion drawn above about the two types of wakes remains tenable.

The flow patterns generated by the fast and very fast turns have thrust jets, whereas the flow patterns without thrust jet appear frequently in the slow and moderate turns. The wake type of a routine single-beat turn probably depends on the recoil

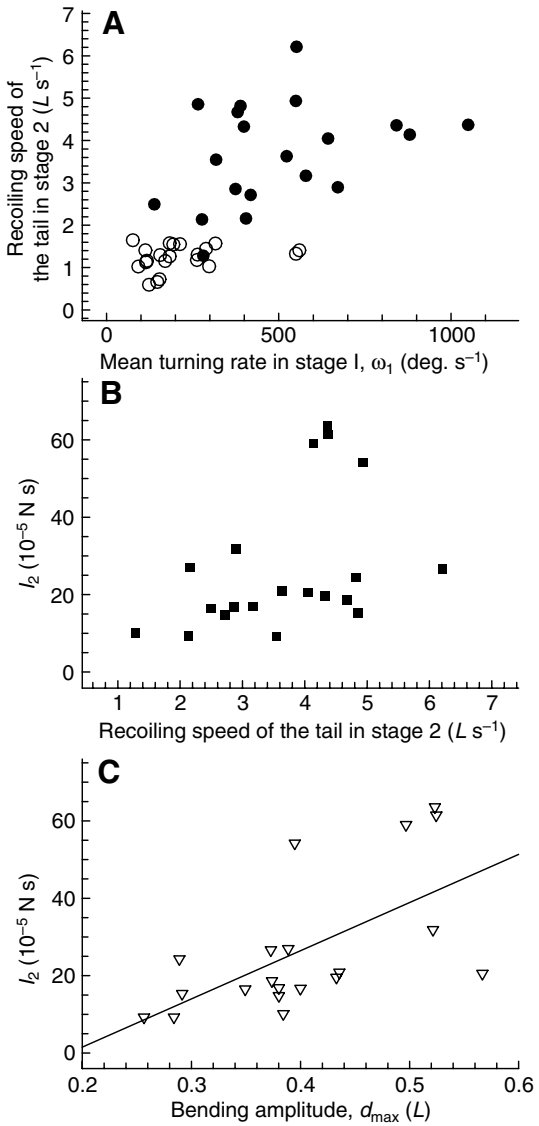

Fig. 8. (A) Scatter plot of the recoil speed of the tail in stage 2 against the mean turning rate in stage 1 (ω_1). Filled circles, turns with type I wake; open circles, turns with type II wake. (B) Scatter plot of the momentum of the vortex ring shed in stage 2 (I_2) against the recoil speed of the tail in stage 2. (C) Linear regression of I_2 against the bending amplitude (d_{max}).

speed of the tail in stage 2. It seems that when the recoil speed of the tail is greater than a critical value (in the present study, it is $2\,L\,s^{-1}$), wake type I appears; otherwise, wake type II appears (Fig. 8A). Unfortunately, there is an exception to this rule. (As shown in Fig. 8A, in one turn, the recoil speed of the tail is $1.3\,L\,s^{-1}$, but it generates the wake of type 1.) Moreover, although the momentum I_2 seems to increases with recoil speed of the tail (Fig. 8B), the correlation between them is not significant (r^2=0.171, P=0.07). Therefore, although the carp can control the recoil speed of the tail to influence the flow patterns substantially, the recoil speed should not be the only factor that affects the flow patterns, and the bending amplitude is probably another one, because it determines the recoil amplitude of the body and tail in stage 2. They show significant differences between the turns with the two wake types (P<0.001; Table 2). Furthermore, the momentum I_2 increases with the bending amplitude significantly (r^2=0.38, P=0.004; Fig. 8C). However, the bending is accomplished in stage 1, so that by stage 2 the carp cannot control the bending amplitude to control the flow patterns. The angle of attack of the tail is another potential factor that the carp can control to influence the flow patterns. Just as Bainbridge suggested, the angle of attack of the tail is an essential factor determining the magnitude of thrust (Bainbridge, 1963). In the present study, although ϕ_{2b} shows no significant difference between the turns with the two types of wakes, the significant differences in ϕ_{2m} and ϕ_{2e} between the two types of turns (Table 2) indicate that in stage 2, the mean angles of attack of the tail in the turns with wake type I are substantially greater than those in the turns of wake type II. It seems that the greater angle of attack of the tail, the more likely the carp will generate thrust jet in stage 2 of a turn. On the other hand, it is necessary to realize that the angles of attack of the tail are different for different regions. Moreover, when the tail flicks, it performs a complex three-dimensional motion (Lauder, 2000). Therefore, more detailed three-dimensional kinematics of the tail is necessary for examining the effects of tail motion on the generated flow patterns.

Center of mass

It is difficult to obtain the real COM of a fish when it performs a turning maneuver. Several investigators (Webb, 1976; Domenici and Blake, 1991; Domenici et al., 2004) assumed the COM of a stretched-straight body is the same as that of a bent body, namely, the COM is always at a fixed position on the midline (typically, 0.33–0.39 L from the nose). Obviously, however, the COM of a fish will move away from the midline when the fish bends its body. Additionally, the more tightly the fish bends, the more substantial the error is in the estimation of the COM. In the present study, the density of fish is assumed to be homogeneous and the geometric center is used instead of the COM. The geometric centers for the stretched-straight carp in our experiments are on the midline, at 0.35–0.37 L from the nose. They are close to the results reported for the COM values of fishes that have similar body shape to koi carp (Webb, 1975; Webb, 1976). It seems that using the geometric center instead of the COM in the present study is acceptable. Furthermore, geometric center should be more precise than a fixed point on the midline of a fish in estimating the COM for studying of turning maneuvers of fish.

Concluding remarks

In routine single-beat turns of koi carp, the turning angle in stage 1 accounts for the greatest portion of the total turning angle. The durations of stage 1 remain relatively stable over a nearly tenfold change in turning rate. Consequently, the turning angle is dominated by the turning rate in stage 1. The turning radius is not related to the swimming speed. Moreover, except in very fast turns, the turning radius is also not affected by the turning rate.

The angle between the side jet and the carp's initial orientation of a turn is always close to 90°, substantially independent of the increasing turning rate. Thus the orientation of the side jet in the forthcoming turn can be predicted. The angle between the jet and the line joining the COM of the carp and the trailing edge of the tail (mean value in stage 1) is also always close to 90°. It is helpful for the carp to maximize the torque so as to improve the turning efficiency. In stage 1, the impulsive moment obtained from the beat of the body and tail and the mean angular momentum of the carp show an agreement in magnitude.

Two types of flow patterns are found in the wake of routine single-beat turns. The difference between the two types of wakes is whether or not a vortex ring and the thrust jet are generated in stage 2. The recoil speed of the tail, the bending amplitude of the turn, and the angle of attack of the tail are three probable factors influencing the flow patterns in stage 2.

List of symbols and abbreviations

a	major axis of the ellipsoid used to model the body of a carp
b	minor axis of the ellipsoid used to model the body of a carp
BCF	body and/or caudal fin
c	vertical semi-minor axis used to model the body of a carp
COM	center of mass
d	lateral excursion of the tail tip
D	diameter of the vortex ring in the plane of the light sheet
d_{max}	maximum value of lateral excursion of the tail tip (bending amplitude)
DPIV	digital particle image velocimetry
h	height of the vortex ring
I	momentum of a vortex ring (general)
I_1	momentum of the vortex ring shed in stage 1
I_2	momentum of the vortex ring shed in stage 2
J	moment of inertia of a carp (general)
J_1	mean moment of inertia of a carp in stage 1
J_a	added moment of inertia of entrained liquid (general)
J_{a1}	mean added moment of inertia of entrained liquid in stage 1
k	coefficient of added moment of inertia of entrained liquid
l_c	distance between the COM of a carp and the trailing edge of the tail (mean value in stage 1)
L	body length of the fish
L_{i1}	impulsive moment obtained from the beat of the body and tail in stage 1

L_{j1}	mean angular momentum of a carp in stage 1
MPF	median and/or paired fin
R_t	turning radius of a carp
t_1	duration of stage 1
t_2	duration of stage 2
U_0	moving speed of a carp at the onset of a turn
x', y'	Cartesian coordinates of a turning carp
α	jet angle of a vortex ring (general)
α_1	jet angle of the vortex ring shed in stages 1
α_2	jet angle of the vortex ring shed in stages 2
β	turning angle of a carp (general)
β_1	turning angle of a carp in stage 1
β_2	turning angle of a carp in stage 2
ΔU_1	net change of speed in stage 1
ΔU_2	net change of speed in stage 2
ϕ_{2b}	angle of attack of the tail at the beginning of stage 2 (only for the tail tip)
ϕ_{2m}	angle of attack of the tail at the middle of stage 2 (only for the tail tip)
ϕ_{2e}	angle of attack of the tail at the end of stage 2 (only for the tail tip)
Γ	circulation of single vortex
$\bar{\Gamma}$	the mean absolute value of the circulations of a pair of vortices
θ	angle between the jet and the line through the COM of the carp and the trailing edge of the tail (mean value in stage 1)
ρ	density of fresh water
ω_1	mean turning rate of a carp in stage 1
ω_2	mean turning rate of a carp in stage 2

We thank Dr L. Li for his help in improving the English in our paper. Two anonymous reviewers contributed greatly to the manuscript. This work is supported by National Natural Science Foundation of China 10332040.

References

Bainbridge, R. (1963). Caudal fin and body movements in the propulsion of some fish. *J. Exp. Biol.* **40**, 23-56.

Brackenbury, J. (2003). Escape manoeuvres in damsel-fly larvae: kinematics and dynamics. *J. Exp. Biol.* **206**, 389-397.

Budick, S. A. and O'Malley, D. M. (2000). Locomotor repertoire of the larval zebrafish: swimming, turning and prey capture. *J. Exp. Biol.* **203**, 2565-2579.

Dabiri, J. O. (2005). On the estimation of swimming and flying forces from wake measurements. *J. Exp. Biol.* **208**, 3519-3532.

Domenici, P. and Blake, R. W. (1991). The kinematics and performance of the escape response in the angel fish (*Pterophyllum eimekei*). *J. Exp. Biol.* **156**, 187-205.

Domenici, P. and Blake, R. W. (1997). Fish fast-start kinematics and performance. *J. Exp. Biol.* **200**, 1165-1178.

Domenici, P., Standen, E. M. and Levine, R. P. (2004). Escape manoeuvres in the spiny dogfish (*Squalus acanthias*). *J. Exp. Biol.* **207**, 2339-2349.

Donley, J. M. and Dickson, K. A. (2000). Swimming kinematics of juvenile kawakawa tuna (*Euthynnus affinis*) and chub mackerel (*Scomber japonicus*). *J. Exp. Biol.* **203**, 3103-3116.

Drucker, E. G. and Lauder, G. V. (2000). A hydrodynamic analysis of fish swimming speed: wake structure and locomotor force in slow and fast labriform swimmers. *J. Exp. Biol.* **203**, 2379-2393.

Drucker, E. G. and Lauder, G. V. (2001). Wake dynamics and fluid forces of turning maneuvers in sunfish. *J. Exp. Biol.* **204**, 431-442.

Ferry, L. A. and Lauder, G. V. (1996). Heterocercal tail function in leopard sharks: a three-dimensional kinematic analysis of two models. *J. Exp. Biol.* **199**, 2253-2268.

Fincham, A. M. and Spedding, G. R. (1997). Low cost, high resolution DPIV for measurement of turbulent fluid flow. *Exp. Fluids* **23**, 449-462.

Gerstner, C. L. (1999). Maneuverability of four species of coral-reef fish that differ in body and pectoral-fin morphology. *Can. J. Zool.* **77**, 1102-1110.

Jayne, B. C. and Lauder, G. V. (1995). Speed effects on midline kinematics during steady undulatory swimming of largemouth bass, *Micropterus salmoides*. *J. Exp. Biol.* **198**, 585-602.

Lauder, G. V. (2000). Function of the caudal fin during locomotion in fishes: kinematics, flow visualization, and evolutionary patterns. *Am. Zool.* **40**, 101-122.

Milne-Thompson, L. M. (1966). *Theoretical Aerodynamics*. New York: Macmillan.

Mori, N. and Chang, K. (2004). Introduction to MPIV-PIV toolbox in MATLAB- version 0.965. http://sauron.urban.eng.osaka-cu.ac.jp/~mori/softwares/mpiv.

Müller, U. K., Van Den Heuvel, B. L. E., Stamhuis, E. J. and Videler, J. J. (1997). Fish foot prints: morphology and energetics of the wake behind a continuously swimming mullet (*Chelon labrosus* Risso). *J. Exp. Biol.* **200**, 2893-2906.

Müller, U. K., Smit, J., Stamhuis, E. J. and Videler, J. J. (2001). How the body contributes to the wake in undulatory fish swimming: flow fields of a swimming eel (*Anguilla anguilla*). *J. Exp. Biol.* **204**, 2751-2762.

Nauen, J. C. and Lauder, G. V. (2002). Hydrodynamics of caudal fin locomotion by chub mackerel, *Scomber japonicus* (Scombridae). *J. Exp. Biol.* **205**, 1709-1724.

Sakakibara, J., Nakagawa, M. and Yoshida, M. (2004). Stereo-PIV study of flow around a maneuvering fish. *Exp. Fluids* **36**, 282-293.

Saunders, H. E. (1957). *Hydrodynamics in Ship Design*. New York: The Society of Naval Architects and Marine Engineers.

Spierts, I. L. and Leeuwen, J. L. (1999). Kinematics and muscle dynamics of C- and S-starts of carp (*Cyprinus carpio* L.). *J. Exp. Biol.* **202**, 393-406.

Tytell, E. D. (2004). The hydrodynamics of eel swimming. II. Effect of swimming speed. *J. Exp. Biol.* **207**, 3265-3279.

Tytell, E. D. and Lauder, G. V. (2004). The hydrodynamics of eel swimming. I. Wake structure. *J. Exp. Biol.* **207**, 1825-1841.

Walker, J. A. (2000). Does a rigid body limit maneuverability? *J. Exp. Biol.* **203**, 3391-3396.

Webb, P. W. (1975). Acceleration performance of rainbow trout *Salmo gairdneri* and green sunfish *Lepomis cyanellus*. *J. Exp. Biol.* **63**, 451-465.

Webb, P. W. (1976). The effect of size on fast-start performance of rainbow trout *Salmo gairdneri*, and a consideration of piscivorous predator-prey interaction. *J. Exp. Biol.* **65**, 157-177.

Webb, P. W. (1983). Speed, acceleration and manoeuvrability of two teleost fishes. *J. Exp. Biol.* **102**, 115-122.

Webb, P. W. (1991). Composition and mechanics of routine swimming of rainbow trout, *Oncorhynchus mykiss*. *Can. J. Fish. Aquat. Sci.* **48**, 583-590.

Webb, P. W. (1998). Swimming. In *The Physiology of Fishes* (ed. D. H. Evans), pp. 3-24. Boca Raton: CRC Press.

Webb, P. W. and Fairchild, A. G. (2001). Performance and maneuverability of three species of teleostean fishes. *Can. J. Zool.* **79**, 1866-1877.

Weihs, D. (1972). A hydrodynamical analysis of fish turning manoeuvres. *Proc. R. Soc. Lond. B Biol. Sci.* **182**, 59-72.

Wolfgang, M. J., Anderson, J. M., Grosenbaugh, M. A., Yue, D. K. P. and Triantafyllou, M. S. (1999). Near-body flow dynamics in swimming fish. *J. Exp. Biol.* **202**, 2303-2327.

Wu, G., Yang, Y. and Zeng, L. (2006). Novel method based on video tracking system for simultaneous measurement of kinematics and flow in the wake of a freely swimming fish. *Rev. Sci. Instrum.* **77**, 114302.

Wu, G., Yang, Y. and Zeng, L. (2007). Kinematics, hydrodynamics and energetic advantages of burst-and-coast swimming of koi carps (*Cyprinus carpio koi*). *J. Exp. Biol.* **210**, 2181-2191.